Interfacial energetics in the TD-nickel and TD-nichrome systems

L. E. MURR

Department of Metallurgical and Materials Engineering, New Mexico Institute of Mining and Technology, Socorro, New Mexico, USA

The absolute (mean) interfacial free energies are measured in thoria-dispersed (2 vol %) (TD)-nickel and the TD-nichrome (Ni-20% Cr) systems at 1200° C utilizing techniques of scanning electron and transmission electron microscopy. Values of particle/matrix interfacial energies for TD-NiCr and TD-Ni were measured at 2300 and 2000 erg cm^{-2} respectively based upon measured values of 2040 and 2200 erg cm^{-2} for the surface free energies for nichrome (80:20 NiCr) and pure nickel respectively, by the method of zero creep and the measurement of grain-boundary groove angles in the electron microscope. Values of 900 erg cm^{-2} and 1040 erg cm^{-2} were measured for the surface and grain-boundary free energies for thoria (ThO$_2$). The particle/matrix adhesive energy for TD-nichrome was measured to be roughly half that for the TD-nickel system based upon the classical interfacial adhesion concept. It is concluded that the apparent difference in particle/matrix interfacial strength between TD-nickel and TD-nichrome results by a more complex mechanism than simple interfacial decohesion involving phase separation.

1. Introduction

The eventual failure of dispersed-phase systems at high temperatures is expected to result primarily from growth of the dispersed particles. Dispersoid stability, while dependent upon a high free energy of formation, can be altered under certain conditions, resulting in coarsening which leads to increasing particle size and interparticle spacing [1-3]. As a consequence of coarsening, dislocations move more easily, resulting in a decrease in strength and a lower recrystallization temperature or time [4]. Coarsening is favoured for a high concentration of diffusing elements for growth in the matrix adjacent to the particles, and a high particle/matrix interfacial energy [1]. The change in particle volume (coarsening) is in fact directly proportional to the particle/matrix interfacial energy [3].

In addition to the dependence of particle coarsening on interfacial energetics, Olsen and Ansell [5] have shown that particle-matrix separation occurs in thoria-dispersed (TD) nickel in tension prior to yielding, while Webster [6]

has demonstrated a similar feature for TD-nichrome as evidenced by voids around the ThO$_2$ particles. Recently, Franklin *et al.* [7] have concluded that TD-nichrome has an interfacial strength between 198 000 and 238 000 psi* as compared with approximately 40 000 psi measured for TD-nickel [8]. These observations also suggest the importance of interfacial energetics in dispersion-hardened systems.

Since there have been no direct measurements of interfacial energetics in a dispersion-hardened system, it was assumed that an effort to perform such measurements in the popular TD-nickel and TD-nichrome systems could have important implications, particularly with regard to particle stability in the physicochemical and mechanical senses. The present study was therefore undertaken with an initial aim of determining whether, in fact, a difference in the matrix/particle interfacial energy existed in the TD-nickel and TD-nichrome systems, and ultimately to measure the absolute interfacial energies associated with these systems.

*10^3 psi = 6.89 N mm^{-2}

2. Experimental and analytical methods
2.1. Direct measurement of relative interfacial energies in TD-nickel and TD-nichrome sheet

As an effective means to measure particle/matrix energetics in the TD-nickel and TD-nichrome systems, it was decided at the outset to attempt to observe equilibrium interfacial geometries directly within these 2-phase systems from which interfacial energy ratios could be measured. It had been observed in previous studies [9] involving transmission electron microscopy that thoria particles in nickel and nichrome matrices were single crystals, and that agglomerated particles were simple polycrystalline aggregates. The implications of this feature are illustrated in Fig. 1 for the present dispersion-strengthened systems which consisted of 2% ThO_2 in a pure nickel matrix and 2% ThO_2 in a nickel-20% chromium matrix. TD-nickel and TD-nichrome were supplied by Fansteel Corporation in the form of stress relief-annealed sheet. Samples of the sheet materials were then annealed in vacuum ($\sim 10^{-6}$ Torr) for 250 h at 1200°C to ensure equilibrium of polycrystalline aggregates of ThO_2 in the matrices. Thin films of TD-nickel and TD-nichrome were prepared by electro-polishing [10], and electron transparent samples were then observed in a Hitachi-Perkin Elmer H.U. 11 or H.U. 200F electron microscope operated at 125 or 200 kV respectively (Fig. 1).

Having established an interfacial equilibrium for ThO_2 particles in the nickel or nichrome matrices, relative interfacial energies could be measured as depicted schematically in Fig. 2 by obtaining high magnification electron micrographs of the particle-aggregate interfacial geometry. Where approximately true dihedral angles can be assured [10], it is observed that

$$\gamma_{gb(ThO_2)} = 2\gamma_{P/M} \cos\left(\frac{\Omega_{P/M}}{2}\right), \qquad (1)$$

where $\gamma_{gb(ThO_2)}$ is the thoria grain-boundary energy, $\gamma_{P/M}$ is the thoria/matrix or particle/matrix interfacial energy, and $\Omega_{P/M}$ is the dihedral angle measured in the nickel or nichrome matrices from electron transmission micrographs. Since for thoria in nickel or nichrome the value of $\gamma_{gb(ThO_2)}$ is the same, the mean values of the particle/matrix interfacial energies in TD-nickel and TD-nichrome can be computed from
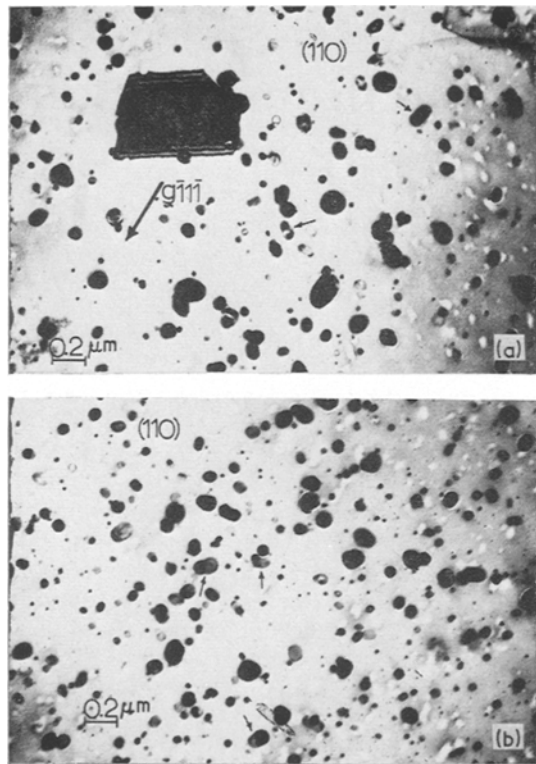
Figure 1 Electron micrographs showing typical annealed TD-nickel (a) and TD-nichrome (b) microstructures. Note the small twin grain in (a) from which the foil thickness can be measured. Note also the apparent decohesion at the particle/matrix interface in a number of cases. Arrows point out ThO_2 crystal aggregates (polycrystals).
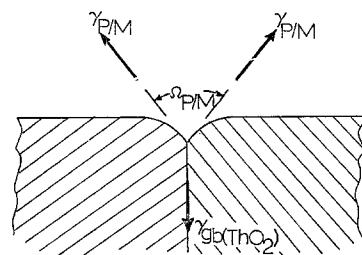
Figure 2 Schematic view of particle/matrix equilibrium at crystal aggregates (polycrystals) and grain boundary/surface intersection equilibrium.

$$\frac{\bar{\gamma}_{P/M(TD-Ni)}}{\bar{\gamma}_{P/M(TD-NiCr)}} = \frac{\cos[\bar{\Omega}_{P/M(TD-NiCr)}/2]}{\cos[\bar{\Omega}_{P/M(TD-Ni)}/2]}, \qquad (2)$$

where $\bar{\Omega}_{P/M(TD-NiCr)}$ and $\bar{\Omega}_{P/M(TD-Ni)}$ are the mean dihedral angles measured for thoria

polycrystalline aggregates in TD-nichrome and TD-nickel respectively.

2.2. Measurement of metal-thoria interfacial energies in the scanning electron microscope

Utilizing the particle-substrate energetic concepts developed by Sundquist [11] and the experimental technique employed by Pilliar and Nutting [12], an attempt was made to equilibrate nickel and nichrome (80:20 NiCr) particles on thoria substrates, and to measure the equilibrium contact angles utilizing the scanning electron microscope as recently described by Murr [13]. Since it has been demonstrated that solid single-crystal metal particles can be equilibrated on a substrate at elevated temperature [11-13], it was decided that the TD-nickel and TD-nichrome interfacial systems could be accurately modelled if single-crystal nickel and nichrome particles could be nucleated and equilibrated on single-crystal thoria substrates at elevated temperature because, as shown in Fig. 1, the TD-nickel and TD-nichrome systems can be considered as single crystal ThO_2 suspended in a single-crystal Ni or NiCr matrix. The energetics of such a system would then appear ideally as shown schematically in Fig. 3, from which it can be observed that at equilibrium (at some fixed temperature)

$$\gamma_{P/M} = F_{S(ThO_2)} + F_{S(M)} \cos \theta_c , \qquad (3)$$

where $\gamma_{P/M}$ is the particle/matrix interfacial energy, $F_{S(ThO_2)}$ is the thoria surface free energy, $F_{S(M)}$ is the metal (or matrix) surface free energy, and θ_c is the contact angle as defined in Fig. 3. It has also been shown that $h/H \cong \cos \theta_c$ [13].
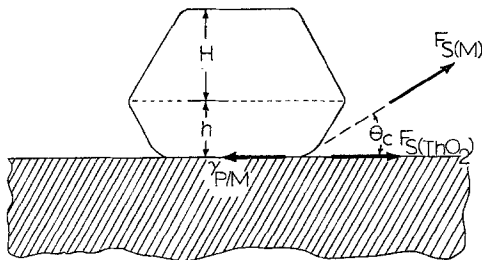
Figure 3 Schematic representation for particle partially wetting a substrate: equilibrium contact angle.

Thoria crystals were synthesized from a ThO_2-Bi_2O_3-PbF_2 flux system previously described by Chase and Osmer [14], consisting of

10, 15, and 75 mol % of the powdered ingredients respectively in a 50 ml platinum crucible. The platinum crucible was heated in an open oven (air) at 1125°C and soaked for 5 h at temperature. Following the initial soaking, the crucible and contents were cooled at a rate of 5° h^{-1} to 950°C and removed from the oven and allowed to air cool. Thoria single-crystal cubes measuring approximately 1 mm on a side were then recovered by digesting the contents of the crucible in hot 50% acetic acid and identified by X-ray diffraction.

The thoria crystals were mounted on small Al_2O_3 coupons using a ceramic paste and inverted in a high vacuum system so that a thin layer of nickel could be vapour-deposited onto the surface of a number of crystals in one case, while a thin layer of nichrome (80:20 NiCr could be vapour deposited in another. Utilizing calibrated weights of pure (99.995%) nickei powder and 80:20 NiCr flakes, roughly 400 Å thick films of each were flash vapour deposited (~ 1000 Å sec^{-1}) onto separate runs of ThO_2 crystals in a vacuum of 2×10^{-6} Torr. Small (5 mm), cleaved (001) single crystals of NaCl were mounted on the same Al_2O_3 coupons as the ThO_2 crystals in order to monitor the vapour deposited films. This was performed by removing the NaCl crystal for each run following vapour deposition and submerging it in distilled water. The nickel or nichrome films which floated on the water were then picked up on standard 200 mesh screen grids and observed in the transmission electron microscope.

Following the successful application of a thin nickel or nichrome film to the ThO_2 crystal surfaces, the crystals-on-coupons were enclosed in small nickel or nichrome boxes, equilibrated in purified hydrogen for 50 h at 1200°C, and furnace cooled. Upon removal from the furnace, individual ThO_2 crystals with equilibrated nickel or nichrome particles attached were observed in a Cambridge Mark II scanning electron microscope operated at 20 kV [13].

2.3. Measurement of absolute interfacial energies in TD-nickel and TD-nichrome

The measurement of interfacial energetics as outlined in Section 2.2. can yield two equations:

$$\left.\begin{array}{l} \gamma_{P/M(TD-Ni)} = F_{S(ThO_2)} \\ \qquad + F_{S(Ni)} \cos \theta_{c(ThO_2-Ni)} \\ \gamma_{P/M(TD-NiCr)} = F_{S(ThO_2)} \\ \qquad + F_{S(NiCr)} \cos \theta_{c(ThO_2-NiCr)} \end{array}\right\} \qquad (4)$$

where $\bar{\theta}_{c(ThO_2-Ni)}$ and $\bar{\theta}_{c(ThO_2-NiCr)}$ are the mean contact angles measured for nickel particles on ThO$_2$ and nichrome particles on ThO$_2$ respectively as shown in Fig. 3. While the thoria surface free energy is unknown, Equation 4 can be solved simultaneously by substituting in Equation 2 for $\gamma_{P/M(TD-Ni)}$ and corresponding values of $F_{S(Ni)}$ and $F_{S(NiCr)}$.

The surface free energies for nickel and nichrome were measured utilizing the zero-creep technique as described previously for these metals [15, 16]. Nickel (99.95%) and nichrome (80 Ni, 20 Cr) wires measuring 5×10^{-6} in. diameter were loaded with a variety of weights of the same material by spot welding small coupon weights onto the wires and suspending a number of wires for each run in a vertical furnace in which the wire samples could be outgassed in vacuum at a temperature of 800°C for 0.5 h. The wires were then crept for 60 h at 1200°C in purified helium. Fiducial marks cut into the wires at 2 cm intervals were utilized in determining the strain-rates, and corresponding plots of strain-rate versus total weight were employed in determining the zero-creep weight, w_0. By measuring the mean wire radius, $\bar{R}$, and the grain length, L, by optical and scanning electron microscopy [15, 16], the zero-creep condition can be expressed experimentally as

$$w_0 g = \pi \bar{R} \left[\bar{F}_{S(M)} - \bar{\gamma}_{gb(M)} \left(\frac{\bar{R}}{L} \right) \right], \quad (5)$$

where g is the gravitational constant for the load w_0 expressed in mg, $\bar{F}_{S(M)}$ is the mean surface free energy, and $\bar{\gamma}_{gb(M)}$ is the mean metal grain-boundary free energy.

By measuring the groove angle where grain boundaries intersect the wire surface as shown schematically in Fig. 2 [15, 16], the grain-boundary free energy, $\gamma_{gb(M)}$ can be determined from Equation 1 in the form

$$\gamma_{gb(M)} = 2F_{S(M)} \cos \left(\frac{\bar{\Omega}_S}{2} \right) \quad (6)$$

where $\bar{\Omega}_S$ is the mean (solid-vapour) dihedral angle measured by direct observations in the transmission electron microscope [15, 16]. Substitution of Equation 6 into Equation 5 then allows the mean surface free energy, $\bar{F}_{S(M)}$ to be determined directly.

3. Results
3.1. Measurement of $\gamma_{P/M(TD-Ni)}/\gamma_{P/M(TD-NiCr)}$
Fig. 4 shows, somewhat typically, the incidence
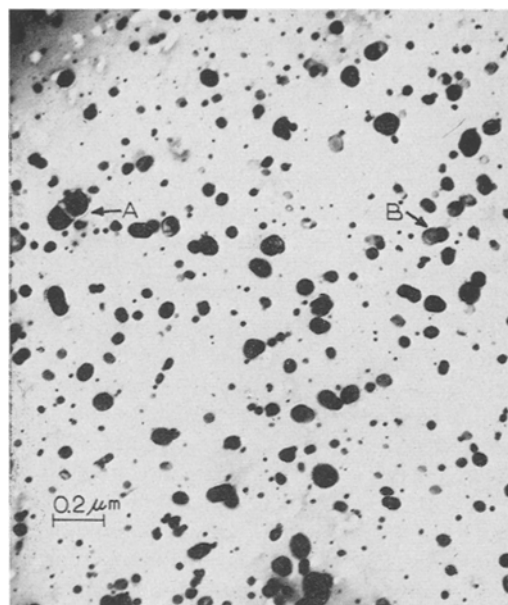
Figure 4 Electron micrograph showing equilibrium ThO$_2$ particle aggregate geometries in TD-nickel. ThO$_2$ bicrystals are indicated at A and B.

of polycrystalline ThO$_2$ aggregates in TD-Ni films and Fig. 5 illustrates the measurement of interfacial dihedral angles at bicrystal and tricrystal aggregates in TD-Ni and TD-NiCr from transmission electron micrographs. Utilizing dark-field techniques [10] as illustrated in Fig. 5d to f, the particle thicknesses could be determined from extinction distance measurements [9], and the true geometries of the dihedral angles reconstructed from the measured boundary inclinations [10, 17, 18] or extinction conditions. The resulting distributions of true dihedral angle measurements for the TD-Ni and TD-NiCr systems are shown in Fig. 6. Mean values of the interfacial dihedral angles determined from the distributions shown in Fig. 6 were $\bar{\Omega}_{P/M(TD-Ni)} = 149.4°$ and $\bar{\Omega}_{P/M(TD-NiCr)} = 153.4°$. Substitution of these values into Equation 2 then resulted in an interfacial energy ratio $\gamma_{P/M(TD-Ni)} : \gamma_{P/M(TD-NiCr)} = 0.87$. As a consequence, the results indicate that the particle/matrix interfacial energy is larger in TD-NiCr than TD-Ni at a temperature of 1200°C.

It should be pointed out that the dihedral angle measurements included in Fig. 6 involved electron micrographs similar to Fig. 5a, b and c where the true dihedral geometry could be
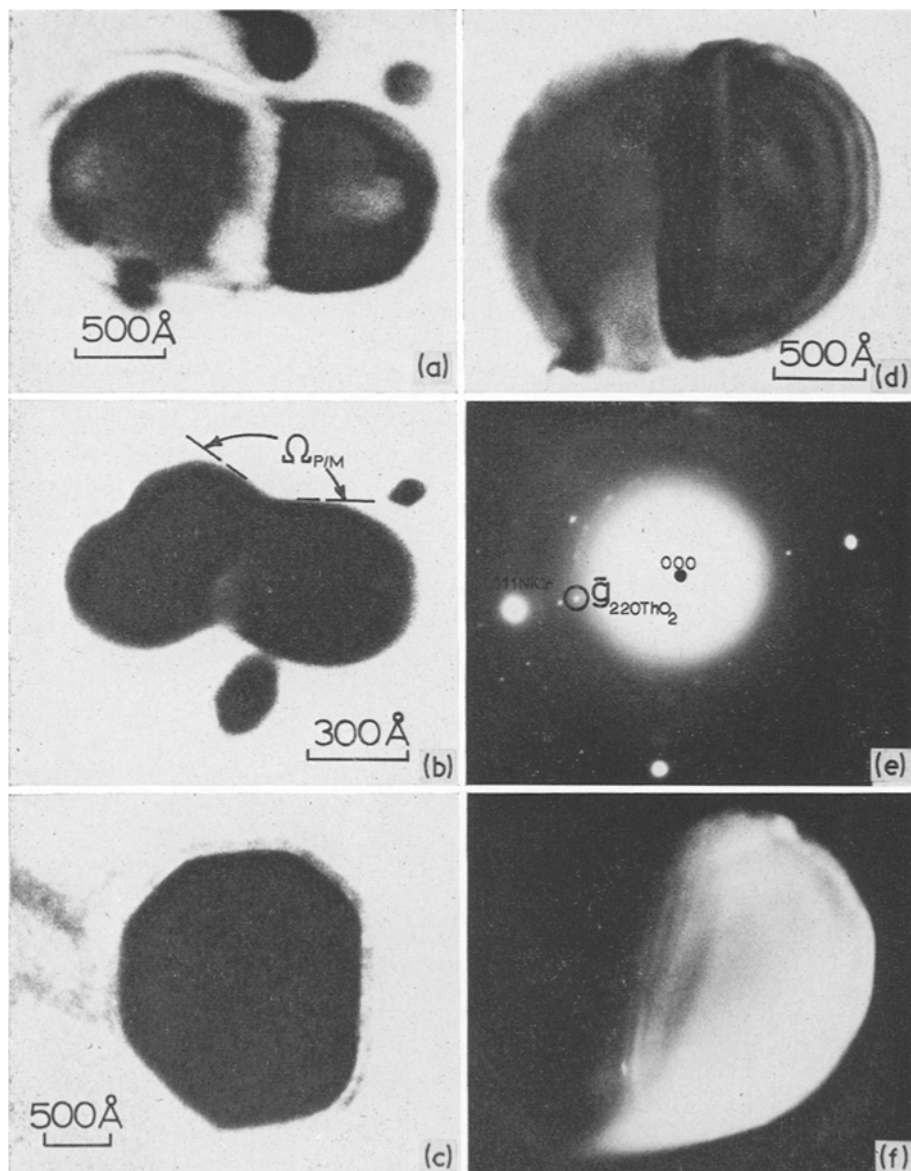
Figure 5 Electron micrographs of equilibrium geometries at ThO₂ particles in TD-nickel and TD-nichrome. (a) Magnified view of ThO₂ bicrystal at A in Fig. 4. (b) ThO₂ tricrystal aggregate in TD-nickel showing dihedral groove angle. (c) Equilibrated (faceted) ThO₂ single crystal in TD-nickel. (d) Bright-field image of ThO₂ bicrystal in TD-NiCr. (e) Selected-area electron diffraction pattern from particle in (d) and surrounding nichrome matrix. (f) Dark-field image of (d) using operating reflection, g, circled in (e) for right grain in (d). Note four extinction fringes characterize the thoria grain boundary. The extinction distance was calculated to be 780 Å at 125 kV.

reasonably assured. Nonetheless, some error is involved in the measurements as implicit in the scatter of dihedral angles shown in Fig. 6. Because of the fact that the ThO₂ particles and the corresponding matrix are crystalline, some of the scatter may also reflect an interfacial energy anisotropy for various crystallographic situations.

The distributions of particle sizes in the as-received (stress-relief annealed) and vacuum

1313

4
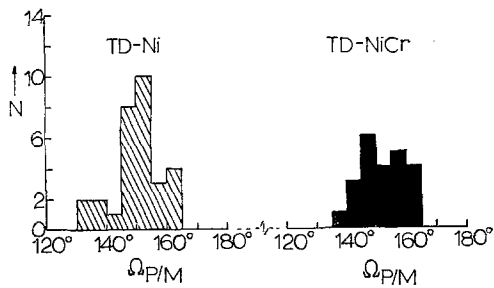
Figure 6 Distribution of particle/matrix dihedral angles, $\Omega_{P/M}$ in TD-nickel and TD-nichrome.

furnace annealed TD-Ni and TD-NiCr sheets are shown in Fig. 7. Each distribution measurement involved a total area of not less than 100 μm²

utilizing transmission electron micrographs similar to those of Figs. 1 and 5. The mean ThO_2 particle diameters were 315 and 340 Å in the as-received and annealed TD-Ni respectively, and 190 and 150 Å in the as-received and annealed TD-NiCr respectively.

3.2. Contact angle measurements for metal particles on thoria substrates

Fig. 8 illustrates the appearance of the flux-synthesized thoria substrates prior to vapour depositing nickel or nichrome films on it. Fig. 9, on the other hand, shows the appearance of the respective thin nickel and nichrome films following vapour deposition (Fig. 9a and c), and the corresponding equilibrated nickel and nichrome particles following furnace anneal in
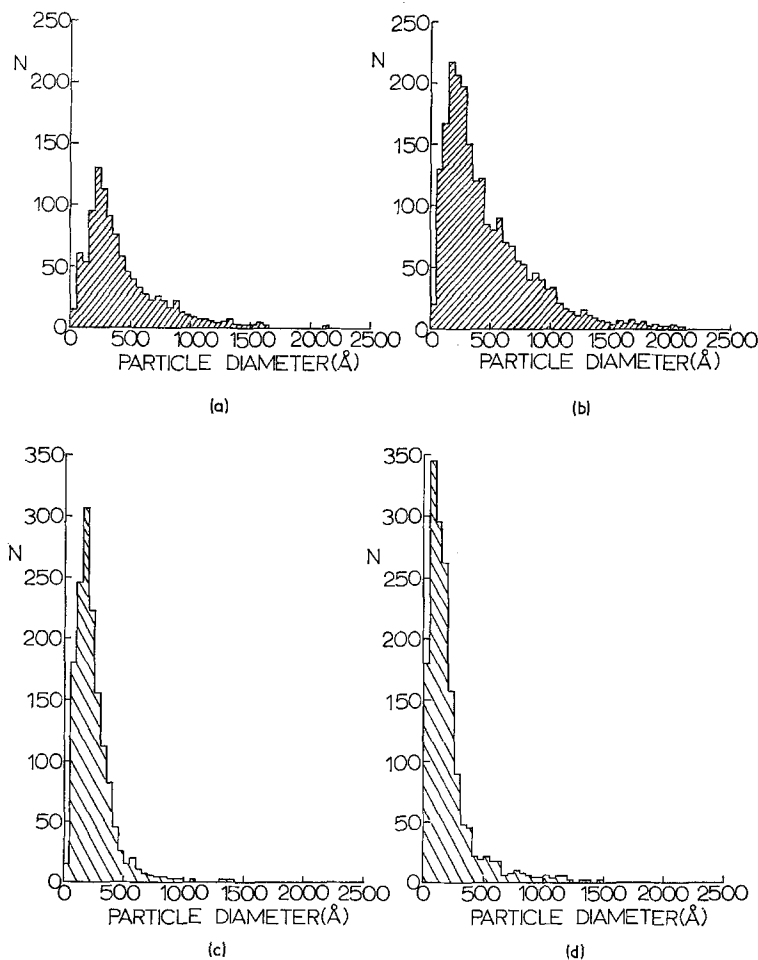
Figure 7 Thoria particle size distributions. (a) Stress-relief annealed (as-received) TD-nickel. (b) Annealed (250 h at 1200°C) TD-nickel. (c) Stress-relief annealed (as-received) TD-nichrome. (d) Annealed (250 h at 1200°C) TD-nichrome.
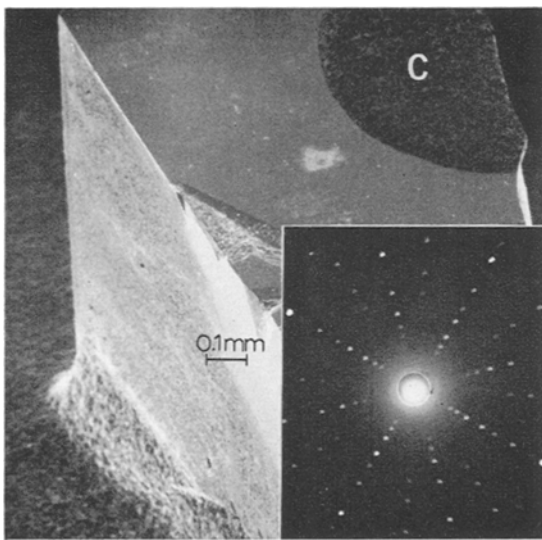
Figure 8 Scanning electron micrograph and super-imposed Läue X-ray diffraction pattern of typical flux grown thoria crystal. C denotes the conducting cement used in mounting the crystal for observation, and also characterize the surface upon which thin films of nickel and nichrome were vapour deposited.

purified hydrogen at 2100°C (Fig. 9b and d). It was necessary, in order to successfully initiate equilibrated particles as shown in Fig. 9b and d, to ensure a more or less discontinuous thin vapour deposit as shown in Fig. 9a and c. While the film structures shown in Fig. 9a and c were extracted from NaCl crystals, the fact that the NaCl surface was the same (001) surface as the ThO_2, having a nearly identical crystal structure, and nearly identical lattice parameter (5.64 Å for NaCl and 5.60 Å for ThO_2) would tend to lend a certain credibility to the implied representation of film structure on the ThO_2.

The contact angles and corresponding shape factors h/H (Fig. 3) were measured for 37 nickel particles on ThO_2 substrates (Fig. 9b) (yielding 74 values of $\theta_{c(ThO_2-Ni)}$) and 34 nichrome particles on ThO_2 substrates (Fig. 9d) (yielding 68 values of $\theta_{c(ThO_2-NiCr)}$). Measured values of $\theta_{c(TD-Ni)}$ ranged from 57° to 70° with a mean value of $\bar{\theta}_{c(ThO_2-Ni)} = 62.6°$ or cos $\bar{\theta}_{c(ThO_2-Ni)} = 0.46$. The corresponding mean value of $\overline{h/H}$ for the nickel-thoria system was found to be 0.54. The cos $\bar{\theta}_{c(ThO_2-Ni)}$ value substituted into Equation 4 was taken as [cos $\bar{\theta}_{c(ThO_2-Ni)} + \overline{h/H}]/2 = 0.50$. Measured values of $\theta_{c(ThO_2-NiCr)}$ ranged from 45° to 61° with a mean value of $\bar{\theta}_{c(ThO_2-N(Cr)} =$

53.2° or cos $\bar{\theta}_{c(ThO_2-NiCr)} = 0.60$. The corresponding mean value of $\overline{h/H}$ for the nichrome-thoria system was found to be 0.70. Consequently, the cos $\bar{\theta}_{c(ThO_2-NiCr)}$ value substituted into Equation 4 was taken as [cos $\bar{\theta}_{c(ThO_2-NiCr)} + \overline{h/H}]/2 = 0.65$.

The stoichiometry of the nichrome particles as shown in Fig. 9d was checked by non-dispersive X-ray spectrometry (using a Princeton-Gamma Tech energy dispersive analysis unit) in the scanning electron microscope and found to vary in composition from 75 to 85% Ni and the balance Cr.

It should also be mentioned that the contact angle measured in the scanning electron microscope was an apparent angle, ω. The correct angle was computed, as described previously by Murr [13] from

$$\theta_c = \tan^{-1}(\tan \omega \sec \phi), \qquad (7)$$

where ϕ denotes the angle of tilt of the ThO_2 substrate in the scanning electron microscope. Since measurements were rarely made for $\phi > 6°$, corrections were generally negligible.

3.3. Nickel and nichrome surface free energies: zero-creep measurements

The results of zero-creep measurements in nickel and nichrome wires are plotted in Fig. 10. The balance load, w_0, for nickel was measured as 25.5 mg, while that for nichrome was 22.0 mg. The mean grain lengths, $\bar{L}$, and corresponding mean wire radii, $\bar{R}$, were measured for nickel and nichrome utilizing an optical metallograph and the scanning electron microscope. Values of the mean dihedral angles, $\bar{\Omega}s$, were also determined from transmission electron shadow-graphs of wire grooves as illustrated in Fig. 11, and the ratio $\gamma_{gb(M)}/F_{S(M)}$ computed from Equation 6. The measured values for $\bar{R}$, $\bar{L}$, w_0 and $\gamma_{gb(M)}/F_{S(M)}$ tabulated in Table I were then substituted into Equation 5 to obtain the corresponding values for $F_{S(Ni)} = 2200$ erg cm^{-2} and $F_{S(NiCr)} = 2040$ erg cm^{-2} at 1200°C.

3.4. Absolute interfacial energies in the TD-Ni and TD-NiCr systems

Substituting the measured values for $F_{S(Ni)}$ and $F_{S(NiCr)}$ and inserting $\gamma_{P/M(TD-Ni)} = 0.87$ $\gamma_{P/M(TD-NiCr)}$ obtained experimentally into Equation 4 results in the two equations with two unknowns: $\gamma_{P/M(TD-NiCr)}$ and $F_{S(ThO_2)}$. Solving simultaneously, $\gamma_{P/M(TD-NiCr)} = 2300$ erg cm^{-2}, and substituting back results in $\gamma_{P/M(TD-Ni)}$
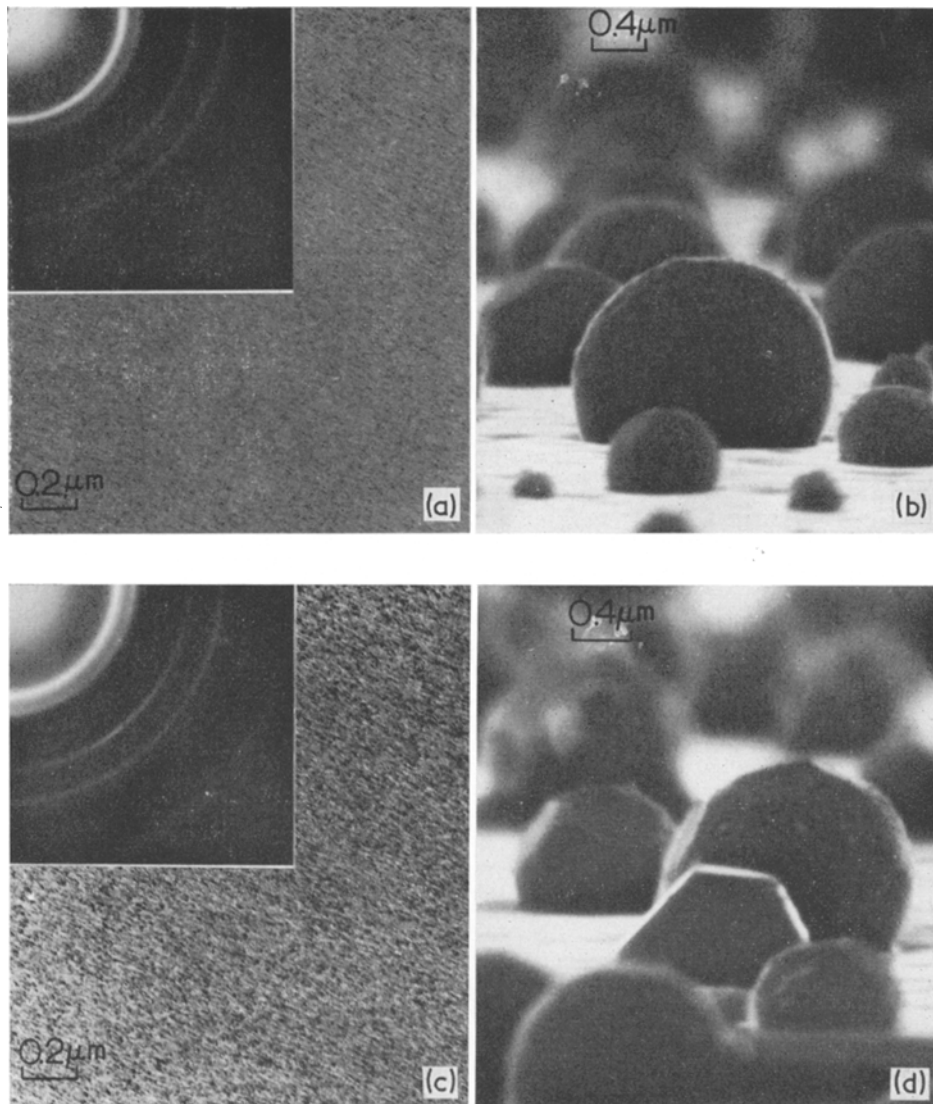
Figure 9 Characterization of vapour-deposited nickel and nichrome films and residual equilibrated metal particles on thoria substrates. (a) Transmission electron micrograph and selected-area electron diffraction pattern of nickel film vapour deposited onto thoria substrates. Note film discontinuities. (b) Scanning electron micrograph showing equilibrated nickel particles on thoria substrate following furnace anneal in hydrogen. (c) Transmission electron micrograph and selected-area electron diffraction pattern of nichrome (80:20 NiCr) film vapour deposited onto thoria substrates. Note film discontinuities. (d) Scanning electron micrograph showing equilibrated nichrome particles on thoria substrate following furnace anneal in hydrogen.

$= 2000$ erg cm^{-2} and $F_{S(ThO_2)} = 900$ erg cm^{-2}. The corresponding thoria grain-boundary energy is then found to be $\gamma_{gb(ThO_2)} = 1040$ erg cm^{-2}.

Table II summarizes the absolute (mean) interfacial energies for the TD-Ni and TD-NiCr

systems measured in this investigation. It is to be noted that the values of the surface free energies, $\bar{F}_{S(Ni)}$ and $\bar{F}_{S(NiCr)}$, are measurements in the pure metal and cannot necessarily be taken to represent the surface (solid alloy-vapour) free

1316
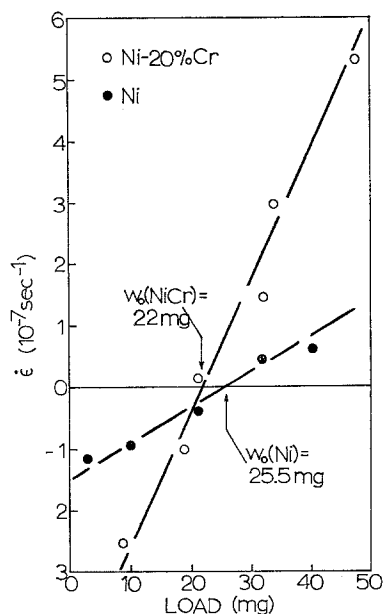
Figure 10 Strain-rate–load graph for nickel and nichrome (80/20 NiCr) wires in helium at 1200° C.
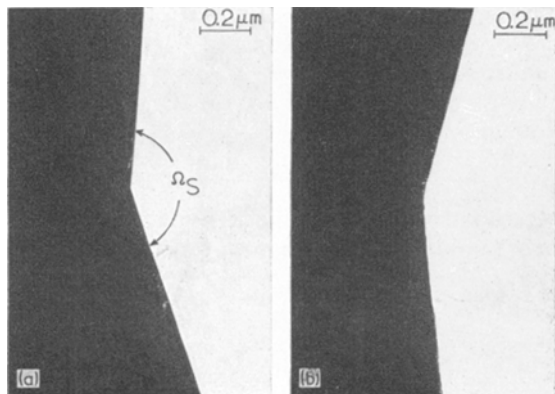
Figure 11 Electron transmission (projection) shadow-graphs of typical grooves formed at the intersection of a grain boundary with the surface of a nichrome wire (a) and a nickel wire (b).

energies for the TD-Ni and TD-NiCr systems. This also applies in the case of the corresponding grain-boundary free energies.

4. Discussion

Although there have been no known attempts to directly measure the solid-solid (particle/matrix) interfacial energies for the Ni-ThO$_2$ or NiCr-ThO$_2$ systems, the Ni-ThO$_2$ value measured in this investigation is comparable with the value of

TABLE I Data of surface and grain-boundary free energy measurements for pure nickel and nichrome at 1200°C

Parameter	Nickel	Nichrome (80:20 NiCr)
Mean linear creep time (h)	60	60
Range of grain lengths Δl (μm)	52–180	55–175
Mean grain length, $\bar{l}$ (μm)	98	90
Range of wire radii, Δr (μm)	39–48	37–43
Mean wire radius, $\bar{r}$ (μm)	43	40
$\bar{r}/\bar{l}$, mean value	0.440	0.444
Zero-creep load, w_0 (mg)	25.5	22.0
Range of groove angles, $\Delta \Omega_S$ (degrees)	145–166	144–166
Mean dihedral groove angle, Ω_S (degrees)	160	159
γ_{gb}/F_S, mean value	0.387	0.362

TABLE II Absolute (mean) interfacial energies in the TD-nickel and TD-nichrome systems at 1200°C

Interfacial energy	TD-nickel	TD-nichrome
Matrix surface free energy ($\bar{F}_{S(M)}$) (erg cm^{-2})	2200	2040
Matrix grain-boundary energy ($\bar{\gamma}_{gb(M)}$) (erg cm^{-2})	840	740
Particle (ThO$_2$) surface free energy ($\bar{F}_{S(ThO_2)}$) (erg cm^{-2})	900	900
Particle (ThO$_2$) grain-boundary energy ($\gamma_{gb(ThO_2)}$) (erg cm^{-2})	1040	1040
Particle/matrix interfacial energy ($\gamma_{P/M}$) (erg cm^{-2})	2000	2300

1510 eg cm^{-2} for an oxygen partial pressure of 10^{-18} atm and 1190 erg cm^{-2} for an oxygen partial pressure of 10^{-14} atm calculated on the basis of diffusion-controlled ThO$_2$ particle growth in TD-Ni at 1350°C by Footner and Alcock [3]. The fact that the values computed by Footner and Alcock are less than the present value would also be expected if the solid-state value of $d\gamma_{P/M}/dT$ is negative as would be expected. On considering the value of $\gamma_{P/M(TD-Ni)}$ = 1510 erg cm^{-2} at 1350°C and the present value, $d\gamma_{P/M(TD-Ni)}/dT \cong -3$ erg cm^2 °C^{-1}. A study is presently underway to measure the temperature coefficient of particle/matrix interfacial energy in the TD-nickel and TD-nichrome systems.

As a check on the measurement of particle/matrix interfacial energy or as an alternative method of measurement, attempts were made to examine the interfacial geometry at ThO$_2$

1317
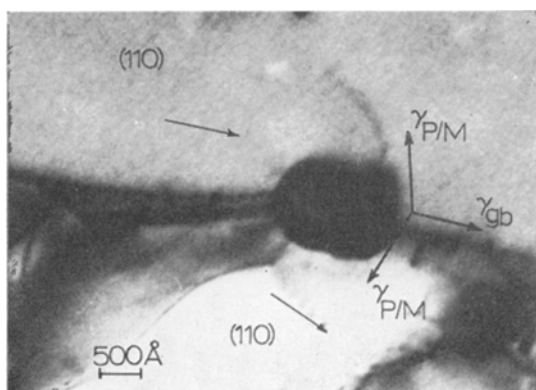
Figure 12 Transmission electron micrograph of thoria particle equilibrated in a grain boundary in TD-nickel. The true dihedral angle [10] in the particle opposite the two grain-boundary intersections (on either side of the particle) averaged 157°. The misorientation of the grain boundary is observed to be 21° as determined by the angle between the [1$\bar{1}$0] directions indicated by the arrows.

particles equilibrated in the grain boundaries of the TD-Ni or TD-NiCr. Only one well-defined instance was observed in TD-NiCr during the course of this investigation for which it was observed that $\gamma_{P/M(TD-NiCr)} \cong 3\gamma_{gb}$. Substituting the value for the grain-boundary free energy for nichrome for γ_{gb} results in a value of $\gamma_{P/M}$ close to the measured value. A good example exhibiting recognizable interfacial geometry for a ThO$_2$ particle in a TD-Ni grain boundary is shown in Fig. 12. The true dihedral angles, computed with a knowledge of the specimen thickness obtained from the extinction condition resulted in $\gamma_{P/M(TD-Ni)} = 2.5 \gamma_{gb}$. Substituting $\bar{\gamma}_{gb} = 840$ erg cm^{-2} obtained for pure nickel (Table II) resulted in a value of 2100 erg cm^{-2} for $\gamma_{P/M(TD-Ni)}$. These observations seem to agree well with the measured values of $\gamma_{P/M}$ despite the fact that the values used for the corresponding grain boundaries were assumed from nickel or nichrome systems and may not be directly applicable in the TD-Ni and TD-NiCr systems.

Franklin, *et al.* [7] have alluded to the fact that a particle/matrix adhesion (interface strength) is greater in the TD-nichrome system by comparison with the TD-nickel system. The energy (or work) of adhesion (or decohesion) can be expressed classically as

$$E_{ad} = F_{S(M)} (1 - \cos \theta_c),\qquad(8)$$

with reference to Fig. 3, or generally,

$$E_{ad} = F_{S(M)} + F_{S(ThO_2)} - \gamma_{P/M}.\qquad(9)$$

On substituting the experimentally determined interfacial energy values into Equation 8 or 9, the particle/matrix adhesive energies for the TD-nichrome and TD-nickel systems are observed to be 640 and 1100 erg cm^{-2} respectively. Strictly speaking this would indicate an opposite trend to that observed [5-7]. However, interface strength as alluded to previously [7] has been related to the stress resulting at the particle/matrix interface by heating to 816 and 982°C and using the equation of Rao *et al.* [19].

In this approach a ThO$_2$ particle of some average (defined) radius is removed from the matrix. Both the matrix void and the particle are then allowed to enlarge as a result of some temperature change. When, ideally, the particle is returned to the void, an elastic distortion occurs which is related to an interfacial stress or strength. The stress results by differences in thermal expansion coefficients, and is intrinsically dependent upon particle radius.

It is, therefore, difficult to assess particle/matrix strength unless the particles have the same size and distribution in the Ni and NiCr matrices. Particle radius is also of primary importance as implicit in the Orowan stress equation

$$\tau_0 = Gb/l,\qquad(10)$$

where l the mean-interparticle spacing, can be expressed in terms of the mean particle radius by [20]

$$l = \bar{r}(1.43V_p^{-\frac{1}{3}} - 1.53)\qquad(11)$$

where V_p is the volume fraction of ThO$_2$ particles; equal to 0.02 in the present investigations. From Fig. 7, the values or r for the annealed TD-Ni and TD-NiCr are observed to be 170 and 75 Å respectively. Consequently, the corresponding interparticle spacings become 1500 and 660 Å respectively for TD-Ni and TD-NiCr. These values are similar to those observed by Franklin, *et al.* [7]. As expected, on substituting for l in Equation 11 into Equation 10, τ_0 (and correspondingly the microhardness) was observed to be greater for TD-NiCr (VHN 321) than for TD-Ni (VHN 215).

While the present results do not support the contention that the particle/matrix adhesion in TD-NiCr is greater than in TD-Ni based upon the classical concept of adhesion as expressed in

Equation 9, it must be emphasized that Equation 9 is predicated upon the classical assumption that interfacial fracture occurs between the two phases, and that no miscibility occurs at the interface. Obviously this is not true.

While no coarsening of ThO_2 particles was observed between the stress-relief annealed (as-received) TD-NiCr and the annealed (250 h at 1200°C) TD-NiCr, the larger particle/matrix interfacial energy measured for TD-NiCr as compared with TD-Ni can be applicable in accounting for the enhanced rate of particle growth in TD-NiCr over TD-Ni observed by Footner and Alcock [3]. In addition, the increased value of the thorium diffusion coefficient in the alloy over the value of pure nickel found by Footner and Alcock [3] can also aid in accounting for a difference in the structure and properties of the particle/matrix interface.

5. Conclusions

The mean (absolute) particle/matrix interfacial energies and associated interfacial free energies have been determined for the first time in the TD-Ni and TD-NiCr systems. The particle-matrix interfacial energy in the TD-Ni system was found to be 0.87 times that in the TD-NiCr system, but the corresponding particle/matrix adhesive energy for the TD-NiCr system was nearly half that for the TD-Ni system based upon the classical concept of interfacial adhesion. These results tend to refute the explanation of differences in particle/matrix interfacial strength in the TD-NiCr and the TD-Ni systems based upon a simple adhesive (or decohesive) concept, and point to a much more complex interfacial system than heretofore envisioned for thoria-dispersed systems in particular, and dispersion-hardened systems in general.

Acknowledgements

References

1. A. W. COCHARDT, *Trans. AIME-J. Metals* **209** (1957) 434.
2. C. B. ALCOCK and P. B. BROWN, *Metal Sci. J.* **3** (1969) 116.
3. P. K. FOOTNER and C. B. ALCOCK, *Met. Trans.* **3** (1972) 2633.
4. F. J. HUMPHREYS and J. W. MARTIN, *Acta Met.* **14** (1966) 775.
5. R. J. OLSEN and G. J. ANSELL, *Trans. ASM* **62** (1969) 711.
6. D. WEBSTER, *ibid* **62** (1969) 936.
7. J. E. FRANKLIN, G. JUDD and G. S. ANSELL, paper 70 in Proceedings of the Third International Conference on Strength of Metals and Alloys, Vol. 1 (August) (1973) and Technical Report 4, Office of Naval Research (October) (1973).
8. R. J. OLSEN, G. JUDD and G. S. ANSELL, *Met. Trans.* **2** (1971) 1353.
9. R. J. HORYLEV and L. E. MURR, "Proceedings of the Electron Microscopy Society of America", edited by C. J. Arceneaux (Claitors, Baton Rouge, La., 1969) p. 168.
10. L. E. MURR, "Electron Optical Applications in Materials Science" (McGraw-Hill, New York, 1970).
11. B. E. SUNDQUIST, *Acta Met.* **12** (1964) 585.
12. R. M. PILLIAR and J. NUTTING, *Phil. Mag.* **16** (1967) 181.
13. L. E. MURR, *Mater Sci. Eng.* **12** (1973) 277.
14. A. B. CHASE, and J. A. OSMEL, *Amer. Mineral.* **49** (1964) 1469.
15. L. E. MURR, R. J. HORYLEV and G. WONG, *Surface Sci.* **26** (1971) 184.
16. L. E. MURR, O. T. INAL and G. WONG, "Electron Microscopy and Structure of Materials", edited by G. Thomas, *et al.* (University of California Press, Berkeley, Calif., 1972) p. 417.
17. L. E. MURR, *Phys. Stat. Sol.* **19** (1967) 7.
18. *Idem, ibid* **25** (1968) 629.
19. G. RAO, R. J. OLSEN, G. JUDD and G. S. ANSELL, *Met. Trans.* **3** (1972) 737.
20. M. H. LEWIS and J. W. MARTIN, *Acta Met.* **11** (1963) 1207.